Thermodynamic models of reactions involving garnet in a sillimanite/staurolite schist

C. T. Foster, Jr.

Department of Geology, University of Iowa, Iowa City, Iowa 52242, USA

ABSTRACT. Textures produced by reactions involving garnet in a sillimanite–staurolite schist have been investigated using an irreversible thermodynamic model. The model predicts that the local production or consumption of garnet is strongly influenced by the proximity of garnet to growing sillimanite and dissolving staurolite. Garnets within sillimanite segregations should dissolve near the sillimanite-bearing centre of the segregation while garnets within or adjacent to staurolite poikiloblasts should grow as the staurolite is replaced by a muscovite-rich pseudomorph. Garnets located in the matrix may grow, not react at all, or dissolve depending on the local configuration of nearby sillimanite, staurolite, and garnet. Textures predicted by the model are similar to those observed in thin section: many garnets are truncated within sillimanite segregations; garnets located in pseudomorphs after staurolite are equant and have thick unpoikilitic rims that suggest growth; most matrix garnets also have thick inclusion-free rims that suggest growth but a few have thin rims, indicating little growth, or are irregularly shaped, suggesting dissolution.

KEYWORDS: garnet textures, garnet–sillimanite–staurolite schist, irreversible thermodynamic models.

MANY textures suggest that metamorphic processes commonly involve local reactions that are linked by material transport through the polygranular matrix of minerals that surrounds the reaction site (e.g. Carmichael, 1969; Joesten, 1974; Yardley, 1977; Bailes and McRitchie, 1978). Interpretation of this type of texture is complicated because a number of reactions could have produced a given texture, depending upon the material transport that took place during the process. A promising approach to this problem is the use of irreversible thermodynamics to calculate reactions that are permitted by material transport through the matrix surrounding the reaction site under local equilibrium conditions (Fisher, 1975, 1977). The stoichiometry of a reaction calculated by this method is dependent upon three factors: (1) the minerals present at the reaction site, (2) the minerals present in the matrix through which diffusion takes place, and (3) the relative values of thermodynamic

diffusion coefficients. The first factor is important because the material transport to and from the reaction site must be a linear combination of the minerals actually present. The second factor provides relations among the chemical potential gradients in the matrix around the reaction site because local equilibrium with the matrix minerals must be maintained. The third factor provides the link between the chemical potential gradients in the matrix and material transport through the matrix to the reaction site. These three constraints can be related to each other in a set of material balance equations that can be solved for reaction stoichiometry, relative chemical potential gradients that are the driving forces for material transport, and mineral modes in the textures produced. The information required for the calculation is a set of relative thermodynamic diffusion coefficients and a specified initial configuration of minerals at both the reaction site and in the matrix surrounding the reaction site. Provided that the relative diffusion coefficients are known, this method allows calculation of a unique set of local reactions for each specified initial configuration of minerals. The textures predicted by the calculated reactions can be quantitatively compared with those observed in rocks, permitting the model to be evaluated. In some cases, the calculations will predict unrecognized textural relations that may be used as additional tests. When relative diffusion coefficients are not available, they may be estimated from some of the observed textures in a rock and then tested against other textures that were not used to obtain the coefficients. Reaction mechanisms responsible for several textures have been satisfactorily explained by models of this type (Fisher, 1977; Joesten, 1977; Foster, 1981, 1982, 1983; Nishiyama, 1983). Although the method has not been widely applied, it has the potential to substantially further our understanding of metamorphic textures and the processes that form them. This paper uses irreversible thermodynamic models to investigate textures formed by local reactions involving garnet

as staurolite breaks down and sillimanite grows in a pelitic schist.

Texture models

The textures discussed in this work are present in the lower sillimanite zone on Elephant Mountain near Rangeley, Maine, USA. They have been previously described by Guidotti (1968) and Foster (1975, 1977). As the grade increases in the lower sillimanite zone, sillimanite grows and staurolite breaks down in rocks containing the assemblage staurolite, garnet, sillimanite, biotite, muscovite, plagioclase, ilmenite, and quartz (Guidotti, 1970, 1974). The most common textures produced by reactions in pelitic rocks within the lower sillimanite zone are: sillimanite segregations composed of a sillimanite-rich core and a biotite-rich/muscovite-free mantle (fig. 1a, upper right); staurolite pseudomorphs composed of abundant muscovite, with
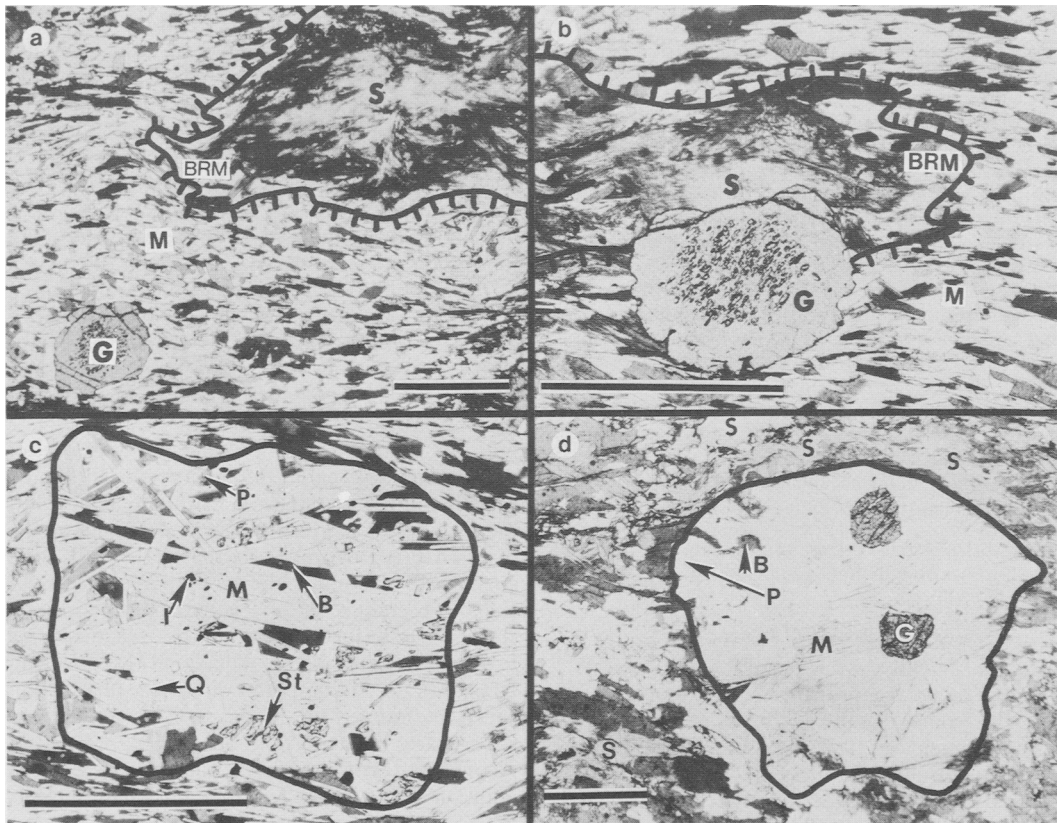
FIG. 1. Photomicrographs. Scale bars are 1 mm long. (a) Garnet-free sillimanite segregation and matrix garnet (G) with an inclusion-free rim. The boundary between the muscovite-bearing matrix (M) and muscovite-free, biotite-rich mantle (BRM) of the sillimanite segregation is marked by a line with ticks on the matrix side. The matrix is composed of muscovite, biotite, plagioclase, ilmenite, and quartz. The biotite-rich mantle has biotite, plagioclase, ilmenite, and quartz present. The sillimanite core (S) is predominantly fibrolite in the centre and a mixture of fibrolite, abundant quartz, minor plagioclase, and biotite at the boundary with the biotite-rich mantle. The boundary between the core and mantle is a dark area in the photomicrographs, primarily due to refraction of light by sillimanite needles in quartz. (b) Garnet-bearing sillimanite segregation. Lines and labels have the same meaning as in (a). Note the sharp truncation of garnet near the sillimanite core/biotite-rich mantle boundary. (c) Garnet-free mica pseudomorph after staurolite (St). It is muscovite-rich (M) but also contains biotite (B), plagioclase (P), ilmenite (I) and quartz (Q). The boundary of the pseudomorph is shown by a solid line. (d) Garnet-bearing mica pseudomorph after staurolite. The pseudomorph has equant garnets (G) and is muscovite-rich (M) with small amounts of plagioclase (P), ilmenite and quartz. Minor biotite (B) is intergrown near the edge of the pseudomorph away from garnets. The outer mantles of sillimanite segregations (S) have grown up to the edge of the pseudomorph, providing a distinct colour contrast that makes the pseudomorph easily visible. The boundary of the pseudomorph is shown by a solid line.

smaller amounts of biotite, plagioclase, quartz, and ilmenite (fig. 1c); and equant garnets with thick inclusion-free rims (fig. 1a, lower left). These three features are separated from each other by a matrix composed of biotite, muscovite, plagioclase, quartz, and ilmenite. Two important variations from the configuration described above appear to be related to the location of garnet relative to sillimanite and staurolite: sillimanite segregations with garnets that are truncated on one side (fig. 1b); and staurolite pseudomorphs that are virtually biotite-free with inclusion-free garnets that have equant shapes (fig. 1d).

Sillimanite segregations. One way to examine the effect of garnet distribution on reaction mechanisms in these rocks is to consider a model where sillimanite nucleates and grows in a matrix of garnet, staurolite, biotite, muscovite, plagioclase, ilmenite, and quartz. The various possible spatial relationships between garnet, sillimanite and staurolite are schematically shown in fig. 2. The configuration shown in the upper part of fig. 2 consists of a garnet-free sillimanite segregation (fig. 1a) and a garnet-free pseudomorph after staurolite (fig. 1c) that are separated by a matrix containing biotite, muscovite, plagioclase, quartz, and ilmenite with isolated garnets. It has been modelled by Foster (1981) as three distinct textures (sillimanite, staurolite, garnet) linked together by material transport between reaction sites. The driving forces for material transport are the chemical potential gradients established when sillimanite nucleates and begins to grow in the matrix surrounding garnet and staurolite. In this paper, Foster's (1981)
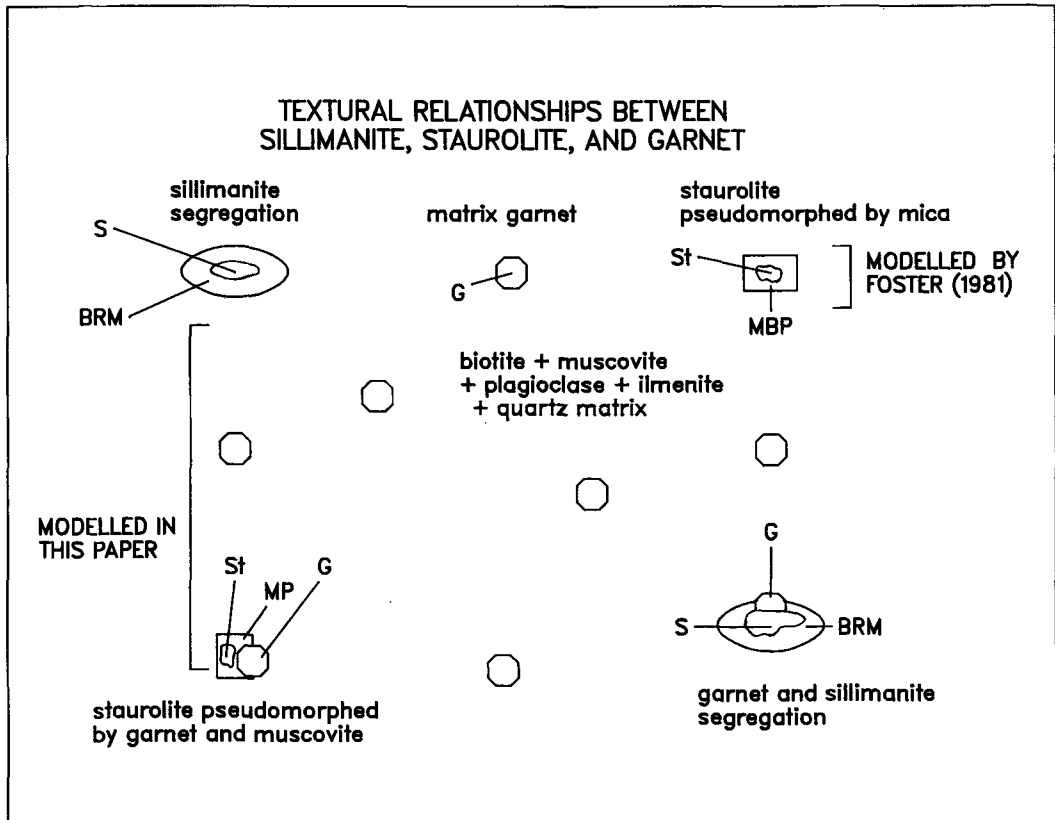
FIG. 2. Textural relationships among staurolite, garnet, and sillimanite in rocks from Elephant Mountain near Rangeley, Maine, USA. The garnet-free sillimanite segregations and garnet-free staurolite pseudomorphs shown in the upper part of the figure were modelled in a previous paper (Foster, 1981). The garnet-bearing sillimanite segregation and garnet-bearing staurolite pseudomorph shown in the lower part of the figure are the subject of the models presented in the paper. S = sillimanite-rich core, BRM = muscovite-free, biotite-rich mantle, G = garnet, St = staurolite poikiloblast, MBP = muscovite-rich, biotite-bearing pseudomorph after staurolite, MP = muscovite-rich, biotite-free pseudomorph after staurolite.

model is extended to include truncated garnets near sillimanite segregations (fig. 1b) and garnet-bearing, biotite-free, muscovite-rich pseudomorphs after staurolite (fig. 1d).

When sillimanite nucleates and begins to grow in a rock containing garnet, staurolite, biotite, muscovite, plagioclase, quartz, and ilmenite, the reaction that can take place between the growing sillimanite and the matrix minerals is calculated by solving the system of equations shown in fig. 3. The derivation of these equations is given by Fisher (1975, 1977) and Foster (1981). The first six rows of the square matrix represent the Gibbs–Duhem constraints on chemical potential gradients in the matrix. These equations are dependent upon the assumption that the matrix minerals are in local equilibrium with chemical potentials along the grain boundaries. The component SiO_2 has been omitted from these equations because the random orientations of micas in staurolite pseudomorphs and fibrolite needles in sillimanite segregations suggest the rock is not under a deviatoric stress during sillimanite growth. Therefore, the presence of free quartz in all domains of the rock fixes the chemical potential of SiO_2 at a constant value throughout the rock. Water is left out of the equations because the chemical potential of H_2O is assumed to be fixed by a water-rich phase along the grain boundaries of the rock. This appears to be a reasonable assumption because the net reaction

taking place in the rock involves production of water. Rows seven through thirteen of the square matrix represent conservation equations that require material transported through the matrix to be produced or consumed by reactions among solid phases in the segregation. The last row balances the reactions for SiO_2 to permit calculation of the amount of quartz produced or consumed by the reaction. The water-rich phase along the grain boundaries serves as a source or sink for H_2O. The mineral compositions and matrix modes used in the model are taken from specimen RA66D2 of Foster (1977), a rock with garnet-free sillimanite segregations, garnet-free staurolite pseudomorphs, garnet-bearing sillimanite segregations, garnet-bearing staurolite pseudomorphs, and garnets not associated with either sillimanite or staurolite. Mn and Zn have been ignored in the minerals because they are present in minor amounts. Test calculations show that minor elements do not substantially affect the material transport predicted by the model. The reference frame for the calculations was chosen to be SiO_2-fixed because it is equivalent to an inert marker reference frame when free quartz is present without a deviatoric stress (see Foster, 1981, p. 265, for discussion). The relative thermodynamic diffusion coefficients (L_i) used in the equations are: FeO = 2.63, $NaO_{0.5}$ = 0.93, MgO = 1.82, $AlO_{1.5}$ = 5.88, $KO_{0.5}$ = 1, CaO = 0.17, and TiO_2 = 0.38 (Foster, 1981). Absolute values for L_i

$$
\begin{bmatrix}
v_{Fe}^{St} & v_{Na}^{St} & v_{Mg}^{St} & v_{Al}^{St} & v_{K}^{St} & v_{Ca}^{St} & v_{Ti}^{St} & 0 & 0 & 0 & 0 & 0 & 0 & 0 \\
v_{Fe}^{G} & v_{Na}^{G} & v_{Mg}^{G} & v_{Al}^{G} & v_{K}^{G} & v_{Ca}^{G} & v_{Ti}^{G} & 0 & 0 & 0 & 0 & 0 & 0 & 0 \\
v_{Fe}^{B} & v_{Na}^{B} & v_{Mg}^{B} & v_{Al}^{B} & v_{K}^{B} & v_{Ca}^{B} & v_{Ti}^{B} & 0 & 0 & 0 & 0 & 0 & 0 & 0 \\
v_{Fe}^{M} & v_{Na}^{M} & v_{Mg}^{M} & v_{Al}^{M} & v_{K}^{M} & v_{Ca}^{M} & v_{Ti}^{M} & 0 & 0 & 0 & 0 & 0 & 0 & 0 \\
v_{Fe}^{P} & v_{Na}^{P} & v_{Mg}^{P} & v_{Al}^{P} & v_{K}^{P} & v_{Ca}^{P} & v_{Ti}^{P} & 0 & 0 & 0 & 0 & 0 & 0 & 0 \\
v_{Fe}^{I} & v_{Na}^{I} & v_{Mg}^{I} & v_{Al}^{I} & v_{K}^{I} & v_{Ca}^{I} & v_{Ti}^{I} & 0 & 0 & 0 & 0 & 0 & 0 & 0 \\
L_{Fe} & 0 & 0 & 0 & 0 & 0 & 0 & -v_{Fe}^{St} & -v_{Fe}^{G} & -v_{Fe}^{B} & -v_{Fe}^{M} & -v_{Fe}^{P} & -v_{Fe}^{I} & 0 \\
0 & L_{Na} & 0 & 0 & 0 & 0 & 0 & -v_{Na}^{St} & -v_{Na}^{G} & -v_{Na}^{B} & -v_{Na}^{M} & -v_{Na}^{P} & -v_{Na}^{I} & 0 \\
0 & 0 & L_{Mg} & 0 & 0 & 0 & 0 & -v_{Mg}^{St} & -v_{Mg}^{G} & -v_{Mg}^{B} & -v_{Mg}^{M} & -v_{Mg}^{P} & -v_{Mg}^{I} & 0 \\
0 & 0 & 0 & L_{Al} & 0 & 0 & 0 & -v_{Al}^{St} & -v_{Al}^{G} & -v_{Al}^{B} & -v_{Al}^{M} & -v_{Al}^{P} & -v_{Al}^{I} & 0 \\
0 & 0 & 0 & 0 & L_{K} & 0 & 0 & -v_{K}^{St} & -v_{K}^{G} & -v_{K}^{B} & -v_{K}^{M} & -v_{K}^{P} & -v_{K}^{I} & 0 \\
0 & 0 & 0 & 0 & 0 & L_{Ca} & 0 & -v_{Ca}^{St} & -v_{Ca}^{G} & -v_{Ca}^{B} & -v_{Ca}^{M} & -v_{Ca}^{P} & -v_{Ca}^{I} & 0 \\
0 & 0 & 0 & 0 & 0 & 0 & L_{Ti} & -v_{Ti}^{St} & -v_{Ti}^{G} & -v_{Ti}^{B} & -v_{Ti}^{M} & -v_{Ti}^{P} & -v_{Ti}^{I} & 0 \\
0 & 0 & 0 & 0 & 0 & 0 & 0 & -v_{Si}^{St} & -v_{Si}^{G} & -v_{Si}^{B} & -v_{Si}^{M} & -v_{Si}^{P} & -v_{Si}^{I} & -v_{Si}^{Q}
\end{bmatrix}
\cdot
\begin{bmatrix}
\nabla\mu_{Fe} \cdot A/R_S \\
\nabla\mu_{Na} \cdot A/R_S \\
\nabla\mu_{Mg} \cdot A/R_S \\
\nabla\mu_{Al} \cdot A/R_S \\
\nabla\mu_{K} \cdot A/R_S \\
\nabla\mu_{Ca} \cdot A/R_S \\
\nabla\mu_{Ti} \cdot A/R_S \\
R_{St}/R_S \\
R_{G}/R_S \\
R_{B}/R_S \\
R_{M}/R_S \\
R_{P}/R_S \\
R_{I}/R_S \\
R_{Q}/R_S
\end{bmatrix}
=
\begin{bmatrix}
0 \\
0 \\
0 \\
0 \\
0 \\
0 \\
v_{Fe}^{S} \\
v_{Na}^{S} \\
v_{Mg}^{S} \\
v_{Al}^{S} \\
v_{K}^{S} \\
v_{Ca}^{S} \\
v_{Ti}^{S} \\
v_{Si}^{S}
\end{bmatrix}
$$

FIG. 3. Matrix equations to solve for chemical potential gradients and reaction coefficients. μ_i is the chemical potential of component i, v_i^j is amount of component i in mineral j, A is the area of a surface surrounding the segregation where the chemical potential gradients are measured, and R_j is the coefficient of mineral j in the reaction. R_j is positive when mineral j precipitates, negative when mineral j dissolves. L_j are relative diffusion coefficients from Foster (1981). The sign convention for transport has been chosen so that components that move away from the centre of a segregation have positive fluxes while those that move towards the centre of the segregation have negative fluxes.

Table I Solutions to matrix equations

S=Sillimanite St=Staurolite G=Garnet B=Biotite M=Muscovite P=Plagioclase Q=Quartz I=Ilmenite

S:BMPQI means S surrounded by B+M+P+Q+I

column #	1	2	3	4	5	6	7	8	9	10	11	12
	S:StGBMPQI	S:GBMPQI	S:BMPQI	S:BPQI	S:BQI	S:QI	S:GBPIQ	S:GBIQ	S:GIQ	St:GBMPQI	St:GMPQI	St:MBPQI
text reaction #	(1)	(2)	(3)	.	.	.	(4)	(6)	(8)	(9)	(10)	.
$\nabla\mu_i \cdot A/R_S$												
i												
FeO	-0.002	-0.062	0.045	-0.095	-0.115	0.000	-0.153	-0.189	-0.204	0.060	0.076	-0.104
$NaO_{0.5}$	-0.014	-0.069	-0.142	-0.245	-0.009	0.000	-0.224	-0.005	0.000	0.054	0.108	0.166
MgO	0.001	0.153	0.049	-0.111	-0.135	0.000	-0.082	-0.095	-0.034	-0.152	0.014	0.007
$AlO_{1.5}$	0.000	0.058	0.105	0.218	0.259	0.340	0.209	0.243	0.255	-0.058	-0.100	-0.129
$KO_{0.5}$	0.002	-0.194	-0.340	-0.185	-0.225	0.000	-0.110	-0.122	0.000	0.196	0.322	0.418
CaO	0.056	-0.072	-0.059	-0.320	-0.005	0.000	-0.350	-0.076	-0.118	0.128	0.165	0.107
TiO_2	0.002	0.059	-0.045	0.091	0.110	0.000	0.147	0.181	0.195	-0.057	-0.073	0.101
R_j/R_S												
j												
B	0.011	0.205	0.061	-0.109	-0.134	.	-0.065	-0.073	.	-0.194	.	0.026
M	-0.011	-0.338	-0.277	.	.	.	.	.	.	0.328	0.202	0.235
P	-0.013	0.046	-0.053	-0.275	.	.	-0.254	.	.	-0.058	0.041	0.093
I	0.006	-0.001	-0.007	0.029	0.035	0.000	0.035	0.042	0.037	0.007	-0.013	0.017
Q	-0.410	0.698	0.538	0.356	-0.287	-1.000	0.407	-0.156	-0.265	-1.109	-1.114	-0.864
S	1.000	1.000	1.000	1.000	1.000	1.000	1.000	1.000	1.000	.	.	.
St	-0.128	.	.	.	.	.	.	.	.	-0.128	-0.128	-0.128
G	0.147	-0.279	.	.	.	.	-0.117	-0.154	-0.247	0.426	0.248	.

are not required because the calculations use the number of moles of sillimanite produced (rather than time) as a measure of reaction progress. Previous work (fig. 6 in Foster, 1983, and unpublished data) has shown that models of this type for textures in amphibolite-facies pelites are relatively insensitive to variation of L_i within one standard deviation of the mean given in fig. 4 of Foster (1981).

The unknown terms in fig. 3 are in the middle matrix. The first seven terms in this matrix are the chemical potential gradients that drive material transport through the matrix surrounding the reaction site. The last seven terms in the middle matrix are the coefficients for the reaction among the minerals at the site of sillimanite growth. The solution to the equations shown in fig. 3 is given in the first column of Table I. The first seven rows of Table I give values of $\nabla\mu_i \cdot A/R_S$ for each component while the last eight rows give the values of R_j/R_S for each mineral taking part in the reaction. The measure of reaction progress used to normalize different local reactions to each other is the amount of sillimanite growth in the rock (R_S). The net reaction among the solid phases when one mole of sillimanite grows in a matrix of staurolite, garnet, biotite, muscovite, plagioclase, quartz, and ilmenite is:

0.128 St + 0.011 M + 0.013 P + 0.410 Q →
      1.0 S + 0.147 G + 0.011 B + 0.006 I.   (1)
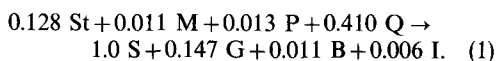
The abbreviations for the minerals in reaction (1) are given at the top of Table I. Examination of the chemical potential gradient terms that drive material transport through the matrix around the reaction site (Table I, col. 1) shows that they are small, indicating the system is essentially closed and requires little exchange with its surroundings.

As sillimanite grows due to reaction (1) it will eventually entirely consume one of the reactant phases, producing a region around the sillimanite that is free of this mineral. The mode of specimen RA66D2 indicates that the first mineral that disappears should be staurolite. When staurolite is eliminated, the chemical potentials in the region around the growing sillimanite are no longer constrained by the Gibbs–Duhem relation of staurolite. The reaction permitted by the remaining phases around the sillimanite can be solved by removing the terms in fig. 3 that involve staurolite (row one of the left matrix, row eight of the centre matrix and row one of the right matrix). The solution to this set of equations is given in col. 2 of Table I. The reaction among the solid phases is:

0.279 G + 0.338 M + 0.001 I →
      1.00 S + 0.205 B + 0.046 P + 0.698 Q.   (2)
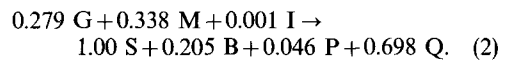
Note that garnet has changed from a product to a reactant phase and that the chemical potential terms indicate there is substantial material transport through the matrix around the sillimanite. Reaction (2) will completely consume one of the

reactant phases in the region around the growing sillimanite, eliminating another Gibbs–Duhem constraint on chemical potentials around the growing sillimanite. The average modes from specimen RA66D2 indicate garnet should be consumed before muscovite or ilmenite. However, because garnet is present as porphyroblasts, there is substantial local variation from the average modes. The critical volume ratio of garnet to muscovite is 1 to 3: if the garnet mode in the vicinity of the sillimanite segregation is less than one-third of the muscovite mode, garnet will be consumed first, forming a garnet-free mantle. If garnet is more abundant than one-third of the muscovite mode, muscovite will be consumed first, forming a muscovite-free mantle containing garnet. Thus, some sillimanite segregations will be garnet-bearing and some will be garnet-free depending upon the abundance of garnet in the vicinity of a given sillimanite segregation.

If garnet is consumed first, the reaction between sillimanite and the remaining phases can be calculated by removing the staurolite and garnet terms from the matrices in fig. 3. The reaction is (Table I, col. 3):

$$0.277 \text{ M} + 0.053 \text{ P} + 0.007 \text{ I} \rightarrow$$
$$1.00 \text{ S} + 0.061 \text{ B} + 0.538 \text{ Q}. \quad (3)$$
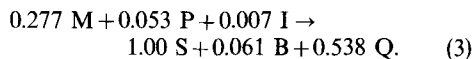
At this stage, the development of the interior of the segregation is the same as the sillimanite segregations discussed by Foster (1982). The solutions for chemical potential gradients and reactions inside of each mantle of a garnet-free sillimanite segregation for the mineral compositions of RA66D2 are given in cols. 3–6 of Table I. The modes in each mantle, reactions between mantles and relative thicknesses of mantles are shown in fig. 4a.

If a garnet lies near the site where sillimanite nucleates, the local muscovite/garnet ratio may fall below 3, allowing reaction (2) to eliminate muscovite before garnet is entirely consumed in the vicinity of the growing sillimanite. Tracings from thin sections illustrating the development of this texture are shown in fig. 5. Note that a segregation with a biotite-rich, muscovite-free mantle is produced and that garnet is truncated near the sillimanite-rich core/muscovite-free mantle boundary.

The local matrix mode used to model this texture is: garnet 50%, biotite 15%, muscovite 16%, plagioclase 3%, ilmenite 2%, and quartz 15%. This mode keeps relative proportions of the matrix minerals other than garnet the same as in the average matrix of RA66D2. The garnet mode was arbitrarily set at 50% to make the muscovite/garnet ratio less than three so that a muscovite-free, garnet-bearing mantle develops. The reaction that

takes place inside the garnet-bearing, muscovite-free mantle around the sillimanite can be obtained by removing the staurolite and muscovite terms from the equations in fig. 3 and solving for the remaining unknowns. The solution is given in the seventh column of Table I. The reaction among the solid phases is:

$$0.117 \text{ G} + 0.065 \text{ B} + 0.254 \text{ P} \rightarrow$$
$$1.00 \text{ S} + 0.407 \text{ Q} + 0.035 \text{ I}. \quad (4)$$
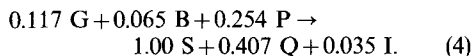
Note that the amount of garnet consumed by the reaction in the portion of the segregation surrounded by the muscovite-free, garnet-bearing mantle is less than in reaction (2). This indicates that a garnet-consuming reaction takes place at the muscovite-free mantle/muscovite-bearing matrix boundary of the sillimanite segregation. The stoichiometry of this reaction is calculated by subtracting reaction (4) from reaction (2):

$$0.162 \text{ G} + 0.338 \text{ M} + 0.035 \text{ I} \rightarrow$$
$$0.269 \text{ B} + 0.300 \text{ P} + 0.292 \text{ Q}. \quad (5)$$
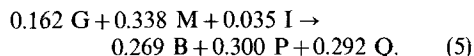
This reaction produces a mantle containing 46% garnet, 29% biotite, 8% plagioclase, 1% ilmenite, 16% quartz. The amount of garnet consumed is relatively small compared with the amount present, making detection of garnet consumption difficult. Reaction (4) will consume plagioclase before biotite or garnet in a mantle with the modes given above, producing a plagioclase-free mantle inside the muscovite-free mantle. The solution to the material transport equations for a plagioclase-free mantle containing garnet, biotite, ilmenite, and quartz is given in the eighth column of Table I. The reaction among the solid phases in the portion of the segregation surrounded by the plagioclase-free/plagioclase-bearing mantle boundary is:

$$0.154 \text{ G} + 0.155 \text{ Q} + 0.073 \text{ B} \rightarrow$$
$$1.000 \text{ S} + 0.042 \text{ I}. \quad (6)$$
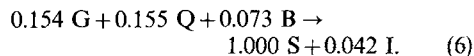
Subtracting reaction (6) from reaction (4) gives the plagioclase-consuming reaction at the plagioclase-bearing/plagioclase-free mantle boundary:

$$0.254 \text{ P} + 0.007 \text{ I} \rightarrow$$
$$0.037 \text{ G} + 0.008 \text{ B} + 0.562 \text{ Q}. \quad (7)$$
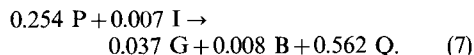
This reaction produces a plagioclase-free mantle with the modes 49% garnet, 30% biotite, 1% ilmenite, 20% quartz. Reaction (6) will eliminate biotite before garnet or quartz in this mantle, forming a biotite-free mantle around the sillimanite. The reaction among the minerals in the sillimanite segregation surrounded by the biotite-free mantle is (Table I, col. 9):

$$0.247 \text{ G} + 0.265 \text{ Q} \rightarrow 1.000 \text{ S} + 0.037 \text{ I}. \quad (8)$$
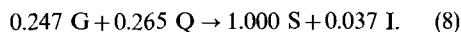
This reaction entirely consumes garnet and much of the quartz, producing a sillimanite-rich core com-
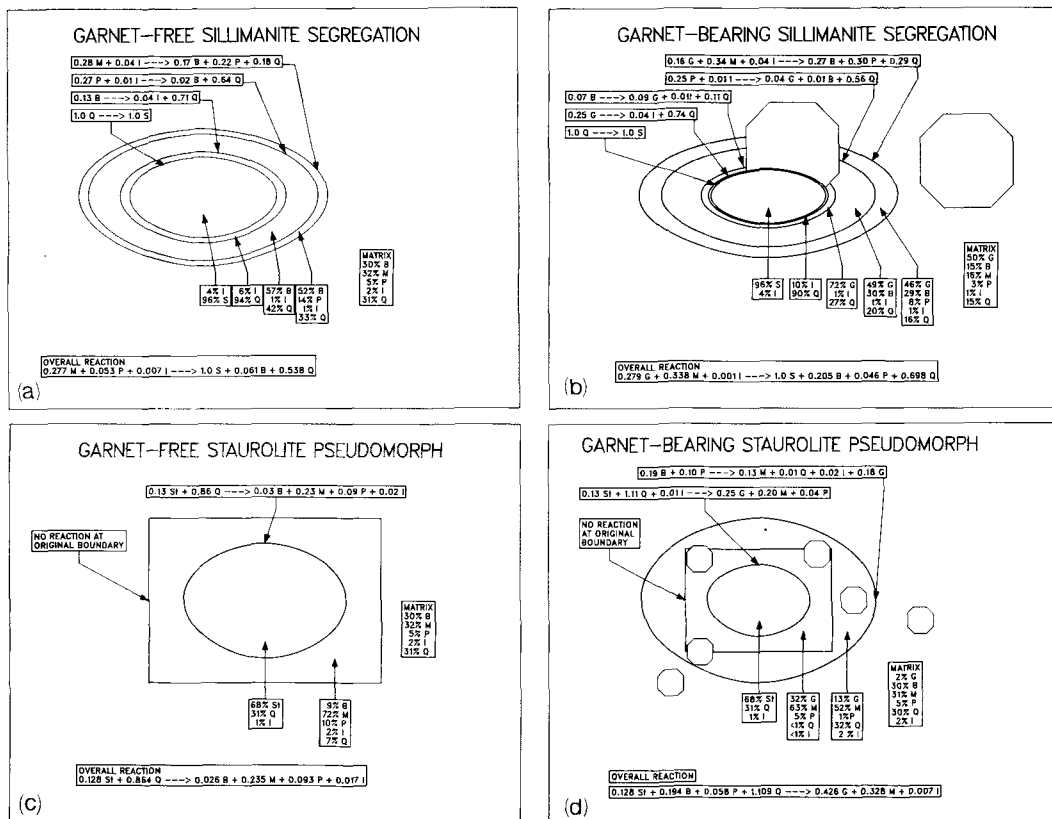
FIG. 4. Calculated reaction models. The net reaction in the segregation or pseudomorph is given in a box at the bottom of each figure. Mineral modes for each region are given above the net reaction. Local reactions are given at the top of each figure. (a) Garnet-free sillimanite segregation produced by sillimanite growth in a matrix composed of 30% biotite, 32% muscovite, 5% plagioclase, 2% ilmenite, and 31% quartz. (b) Garnet-bearing sillimanite segregation produced by sillimanite growth in a matrix composed of 50% garnet, 15% biotite, 16% muscovite, 3% plagioclase, 1% ilmenite, and 15% quartz. (c) Garnet-free staurolite pseudomorph produced by dissolution of a staurolite poikiloblast in a matrix composed of 30% biotite, 32% muscovite, 5% plagioclase, 2% ilmenite, and 31% quartz. (d) Garnet-bearing staurolite pseudomorph produced by staurolite dissolving in a matrix composed of 2% garnet, 30% biotite, 31% muscovite, 5% plagioclase, 2% ilmenite, and 30% quartz.

posed of 87% sillimanite, 8% quartz, and 5% ilmenite. A quartz-rich layer similar to that described by Foster (1981, 1982) may develop between the garnet and sillimanite. The calculated mantle sequence, mantle thickness and mineral modes for a garnet-bearing sillimanite segregation are shown in fig. 4b. The two outer mantles in fig. 4b correspond to the mantle labelled biotite-rich/ muscovite-free in fig. 5. The two inner mantles and centre of the segregation shown in fig. 4b corresponds to the region labelled sillimanite-rich core in fig. 5.

Staurolite pseudomorphs. The segregations discussed in the preceding section grow in staurolite-free regions of the rock because reaction (1)

commonly eliminates staurolite in the vicinity of sillimanite segregations. The type of texture that is produced by the replacement of staurolite is dependent upon the way staurolite is distributed in the rock when sillimanite begins to grow. If staurolite was present as many small crystals that were evenly distributed throughout the rock, reaction (1) would produce a distinct staurolite-free halo around each sillimanite segregation. In this case, the best way to model the texture would be to treat the staurolite-free halo as a mantle around the sillimanite segregation. Another possible configuration would be to have staurolite present as large poikiloblasts. This is the case at Elephant Mountain. Under these circumstances it is most
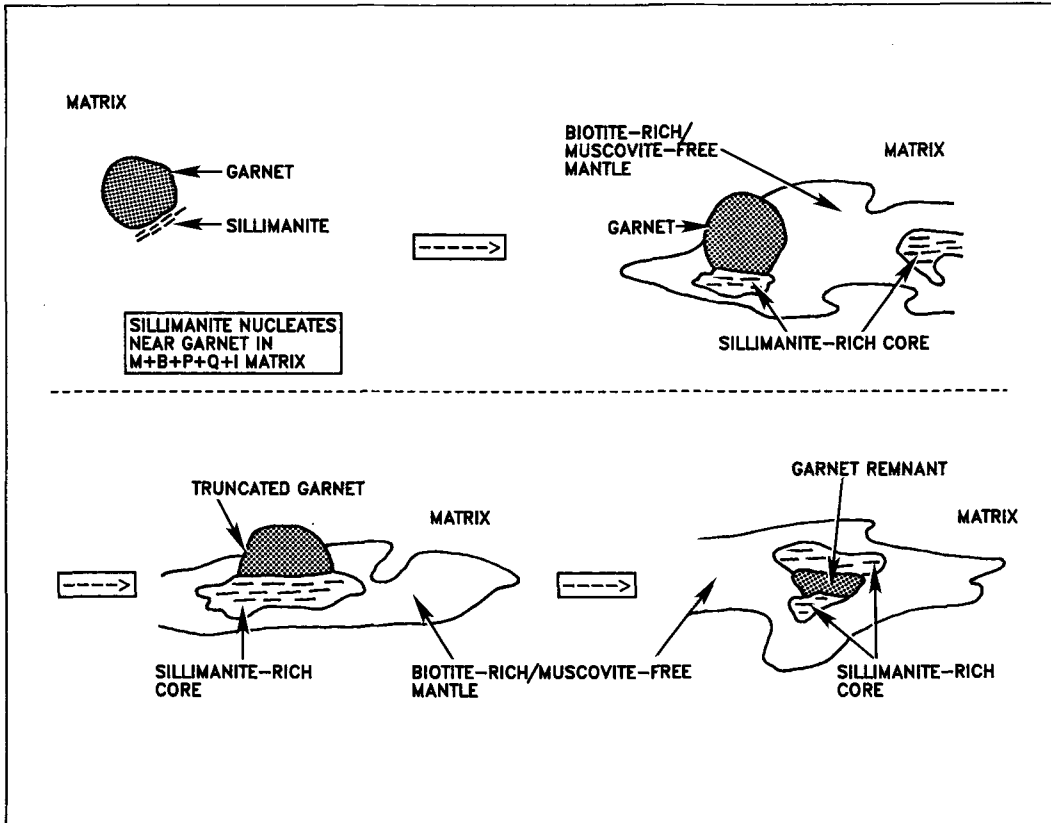
FIG. 5. Tracings from thin sections to show the development of garnet-bearing sillimanite segregations with biotite-rich mantles, sillimanite-rich cores and truncated garnets near the core/mantle boundary.

realistic to model the reactions in the vicinity of staurolite by considering a staurolite poikiloblast dissolving while surrounded by a matrix of garnet, biotite, muscovite, plagioclase, ilmenite, and quartz. The staurolite reaction is linked to the sillimanite reaction by diffusion through the matrix.

The reaction that takes place when a staurolite poikiloblast dissolves in a matrix of garnet, biotite, muscovite, plagioclase, ilmenite, and quartz can be calculated by eliminating the staurolite terms from the left and centre matrix in fig. 3 and then substituting staurolite compositions for sillimanite in the right hand matrix. The chemical potential gradient terms and reaction coefficients for this configuration are given in col. 10 of Table I. The $\nabla\mu_i \cdot A/R_S$ terms are in the first seven rows and the R_j/R_S terms are given in the last eight rows. Note that when reactions involve staurolite as the core mineral (Table I, cols. 10–12), the chemical potential terms and reaction coefficients have been normalized to the amount of sillimanite growth in

the rock, permitting comparison with reactions in sillimanite segregations. Thus, the reaction co-efficient for staurolite (R_{St}/R_S) is −0.128 in cols. 10–12 of Table I because this is the amount of staurolite consumed when one mole of sillimanite grows via reaction (1). The reaction among the solid phases in the vicinity of staurolite when it dissolves is:

$$0.128 \text{ St} + 0.194 \text{ B} + 0.058 \text{ P} + 1.109 \text{ Q} \rightarrow$$
$$0.426 \text{ G} + 0.328 \text{ M} + 0.007 \text{ I}. \quad (9)$$
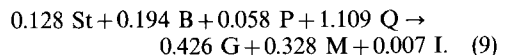
This reaction is different than those discussed above for sillimanite segregations because the reactants are not uniformly distributed. The staurolite and quartz are available in the staurolite poikiloblast but the plagioclase and biotite must come from the region surrounding the poikiloblast. Reaction (9) will eventually completely consume either biotite or plagioclase in the matrix adjacent to the staurolite poikiloblast. For a rock with matrix mineral modes similar to RA66D2, biotite in the matrix would be eliminated before plagioclase.

This causes a biotite-free mantle to develop in the matrix around the staurolite. The reaction in the portion of the pseudomorph surrounded by the biotite-free mantle can be calculated by removing the biotite terms in the staurolite system of equations. The solution is given in col. 11 of Table I. The reaction among the solid phases surrounded by the biotite-free mantle is:

$$0.128 \text{ St} + 1.114 \text{ Q} + 0.013 \text{ I} \rightarrow$$
$$0.248 \text{ G} + 0.202 \text{ M} + 0.041 \text{ P}. \quad (10)$$
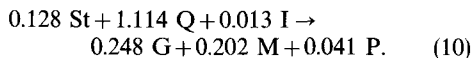
The reaction at the biotite-bearing matrix/biotite-free mantle boundary is obtained by subtracting reaction (10) from reaction (9):

$$0.194 \text{ B} + 0.099 \text{ P} \rightarrow$$
$$0.178 \text{ G} + 0.126 \text{ M} + 0.005 \text{ Q} + 0.020 \text{ I}. \quad (11)$$
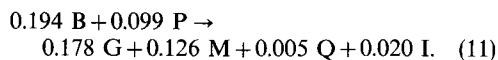
In a rock like RA66D2 this reaction would produce a biotite-free mantle around the staurolite with a composition of 13% garnet, < 1% plagioclase, 52% muscovite, 32% quartz, and 2% ilmenite. Reaction (10) replaces poikiloblasts of staurolite with a pseudomorph of 32% garnet, 63% muscovite, 5% plagioclase, and less than a percent of quartz and ilmenite. Note that reaction (10) migrates from the staurolite poikiloblast/matrix boundary into the staurolite poikiloblast while reaction (9) migrates in the opposite direction, out into the matrix (fig. 4d). The original boundary of the staurolite should be preserved by a change in mineral modes because the portion inside the original boundary was produced by reaction (10) while the outer portion was produced by reaction (11).

A number of minor permutations are possible for this texture depending on the exact proportions of the phases originally present. For example, if plagioclase is not present as inclusions in the staurolite and is unable to nucleate at the reaction interface as reaction (10) proceeds, the pseudomorph would be plagioclase-free and a small amount of plagioclase would be produced at the original boundary of the staurolite poikiloblast. Another variant is possible if the quartz/staurolite ratio in the poikiloblast was low enough so that quartz was entirely consumed before staurolite. Then, the pseudomorph would be quartz-free and the required quartz for reaction (10) would come from the quartz-bearing region at the edge of the pseudomorph. If ilmenite is consumed before staurolite and quartz, an ilmenite-free mantle similar to that described by Foster (1983) would be produced.

The calculated configuration of mantle sequence, modes and mantle thickness for a garnet-bearing staurolite pseudomorph is shown in fig. 4d. This type of pseudomorph is relatively uncommon in Rangeley rocks, apparently because most stauro-lites do not have garnets in close proximity and new garnets do not nucleate during the reaction. In RA66D2, a few mica-rich pseudomorphs partially enclose a single garnet. In these cases, the pseudomorph is commonly biotite-free adjacent to the garnet and the garnet has a thick unpoikilitic rim, suggesting that it grew as staurolite dissolved, in agreement with model calculations. Pseudomorphs that are not biotite-free when garnets are present are plagioclase-free close to the garnet + biotite assemblage, suggesting that a local variation in the matrix biotite/plagioclase ratio may have allowed plagioclase to be eliminated by reaction (9) instead of biotite. The mode change at the original boundary is commonly indistinct because the grain size of the minerals involved in the reaction is about the same as the diameter of the mantle that grows into the matrix. A few rocks have been observed from the top of the lower-sillimanite zone that contain well developed garnet–muscovite pseudomorphs after staurolite (fig. 1d) that resemble the pseudomorph predicted by the calculations (fig. 4d). These rocks are more aluminous than RA66D2 and higher grade, so there has been considerable sillimanite growth and all the staurolite has been consumed. The result is that the outer mantles of the sillimanite segregations are immediately adjacent to the muscovite-rich pseudomorphs after staurolite, making the boundary between the muscovite-free, biotite-rich outer mantle of the sillimanite segregation and the biotite-free, garnet-bearing, muscovite-rich pseudomorph after staurolite easily visible.

Several other types of pseudomorphs after staurolite that are present in the lower sillimanite zone on Elephant Mountain have been discussed by Foster (1983). The most common pseudomorph configuration is one that is muscovite-rich, biotite-bearing, but without garnet. It is produced by staurolite dissolving while surrounded by biotite, muscovite, plagioclase, quartz, and ilmenite. This configuration is shown in figs. 1c and 4c for comparison with the garnet-bearing pseudomorphs (figs. 1d and 4d). The details for its calculation are in Foster (1981).

Garnets. The garnet-bearing layer of biotite, muscovite, plagioclase, ilmenite and quartz that lies between a garnet-free sillimanite segregation (fig. 4a) and garnet-free staurolite pseudomorphs (fig. 4c) would have two distinct reactions taking place if garnet were uniformly distributed in the matrix. The reaction on the sillimanite side would be a garnet-consuming reaction, calculated by subtracting reaction (3) from reaction (2):

$$0.279 \text{ G} + 0.061 \text{ M} \rightarrow$$
$$0.144 \text{ B} + 0.099 \text{ P} + 0.077 \text{ I} + 0.160 \text{ Q}. \quad (12)$$
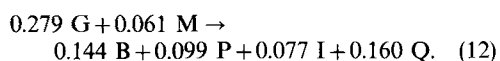
The reaction on the staurolite side would be a garnet-producing reaction calculated by subtracting the overall reaction in the garnet-free pseudomorph (Table I, col. 12) from reaction (9):

$$0.010 \text{ I} + 0.245 \text{ Q} + 0.220 \text{ B} + 0.151 \text{ P} \rightarrow$$
$$0.426 \text{ G} + 0.093 \text{ M}. \quad (13)$$
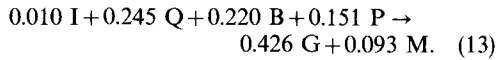
The net reaction taking place in this region can be calculated by adding reaction (12) to reaction (13):

$$0.085 \text{ Q} + 0.003 \text{ I} + 0.052 \text{ P} + 0.076 \text{ B} \rightarrow$$
$$0.032 \text{ M} + 0.147 \text{ G}. \quad (14)$$
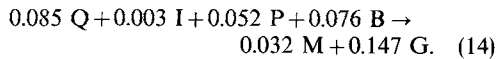
To investigate possible local controls on matrix garnet growth, the models shown in fig. 4 have been combined in a simplified geometry that approximates the relationships observed in rocks from the lower sillimanite zone on Elephant Mountain. This configuration (fig. 6) consists of a sillimanite segregation without garnet, a sillimanite segregation with garnet, a staurolite pseudomorph without garnet, a staurolite pseudomorph with garnet and four garnets away from sillimanite and staurolite. A matrix of biotite, muscovite, plagioclase, ilmenite, and quartz separates the different types of segregations. The overall reaction for each type of staurolite and sillimanite segregation has been shown, but the reactions at individual mantle boundaries have been omitted for simplicity. The reaction stoichiometry has been arbitrarily set so that each sillimanite segregation produces one mole of sillimanite and each staurolite segregation consumes 0.128 moles of staurolite. This produces the same overall reaction stoichiometry for the rock that is given by reaction (1).
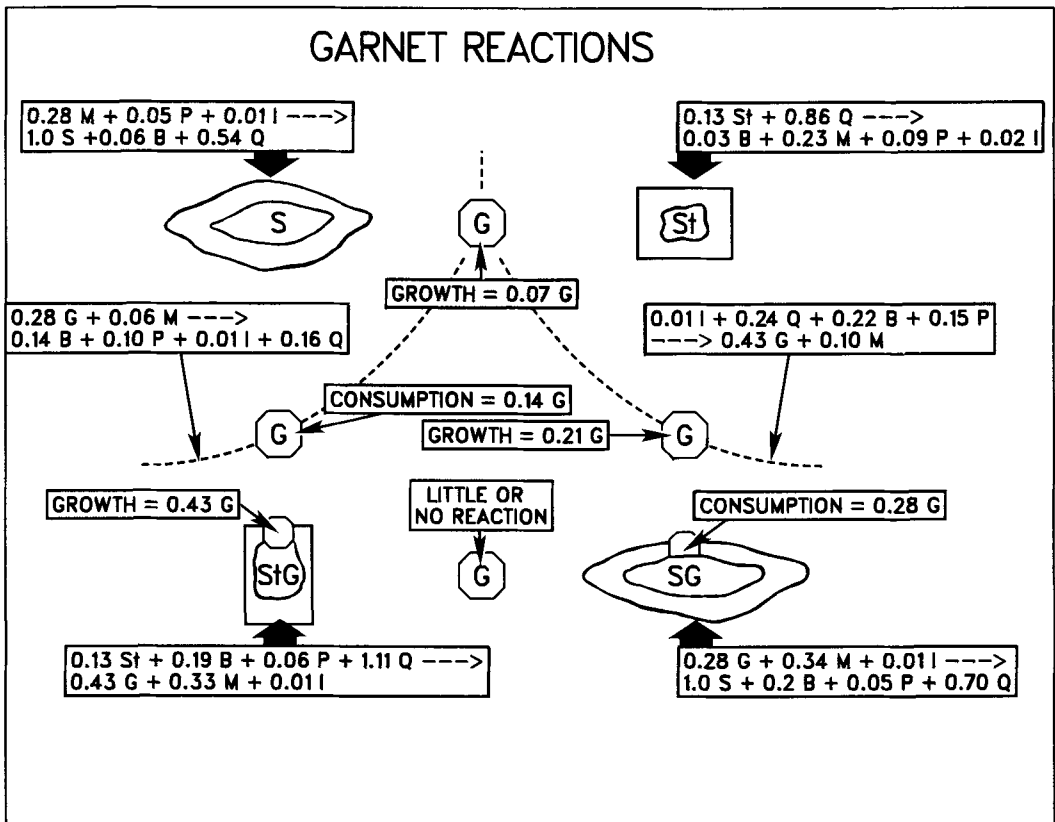
FIG. 6. Schematic configuration of reactions involving garnet in a rock containing both garnet-free and garnet-bearing pseudomorphs and segregations. As discussed in the text, some garnets should grow, some should show little sign of reaction and others should dissolve. The net reaction for each segregation or pseudomorph is given in a box with a bold arrow. The position of reactions (12) and (13) are shown by dashed lines. The amounts of reaction for garnets in different regions of the rock are given in the boxes labelled 'consumption' or 'growth'. The amount of reaction shown for each matrix garnet is half of the stoichiometric coefficient of garnet in the appropriate reaction because consumption or growth has been partitioned between two matrix garnets.

The growth of matrix garnet is primarily influenced by reactions (12) and (13). These reactions should take place when garnet is first encountered around garnet-free sillimanite and staurolite segregations. The positions of these reactions are shown as dashed lines on fig. 6. Note that, depending on its position relative to the other segregations, garnet may dissolve, grow, or not react at all. Consumption of matrix garnets takes place between garnet-free sillimanite segregations and garnet-bearing staurolite pseudomorphs because of reaction (12). Growth of matrix garnets takes place between garnet-bearing sillimanite segregations and garnet-free staurolite pseudomorphs due to reaction (13) and between garnet-free sillimanite and garnet-free staurolite segregations because of reaction (14). Little or no growth takes place in matrix garnets located between garnet-bearing sillimanite segregations and garnet-bearing staurolite pseudomorphs. Garnet reactions also take place within two types of segregations: garnets in the sillimanite/garnet segregation dissolve because of reaction (2) and garnets grow in garnet-bearing staurolite pseudomorphs due to reaction (9).

Examination of garnets in thin sections from the lower sillimanite zone on Elephant Mountain suggests there is variation in the amount of growth that is similar to the model predictions. Garnets within sillimanite segregations appear to have dissolved, producing truncated porphyroblasts (fig. 1b). Garnets within staurolite pseudomorphs are equant and have thick inclusion-free rims, suggesting growth during the replacement of staurolite (fig. 1d). Most matrix garnets appear to have had some growth in the lower-sillimanite zone because they have thick unpoikilitic rims (fig. 1a), a few have thin unpoikilitic rims suggesting little growth, and others have irregular shapes, suggesting they may be dissolving. The spatial relationship of the three types of matrix garnets to sillimanite and staurolite segregations in thin section is consistent with the model, but can not be completely verified because of uncertainty about what was present in the third dimension (perpendicular to the thin sections).

Chemical potential profiles

The primary controls on the reaction mechanisms discussed in the preceding sections are the chemical potential gradients permitted by the Gibbs–Duhem relations for the minerals in the region surrounding the reaction site. Fig. 7 illustrates the relationships of the chemical potentials in the matrix between each type of segregation or pseudomorph shown in fig. 6. The system has been simplified because the gradients have been integrated and plotted as if there were one dimensional diffusion couples

CHEMICAL POTENTIAL PROFILES
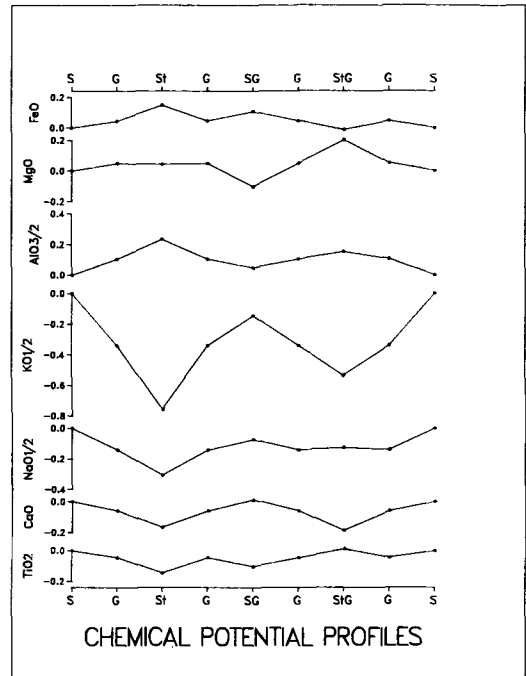
FIG. 7. Profiles showing the relative values of the chemical potential for each component in the matrix between segregations shown in fig. 6. The profile for each component begins at the garnet-free sillimanite segregation (S) in the upper left part of fig. 6 and proceeds in a clockwise direction to the garnet-free staurolite pseudomorph (St), the garnet bearing sillimanite segregation (SG), the garnet bearing staurolite pseudomorph (StG), and finally back to the garnet-free sillimanite segregation (S). Matrix garnets encountered along the path are indicated by G. Profiles within segregations have been omitted for simplicity. The numbers given on the vertical axes are $(\mu_i - \mu_i^0) \cdot A/R_S$. μ_i is the chemical potential of component i along the profile, μ_i^0 is the chemical potential of i at the margin of the garnet-free sillimanite segregation, A is the cross-section area through which diffusion is taking place and R_S is the amount of sillimanite growth.

between the segregations. The chemical potential gradients were obtained from the chemical potential terms given in cols. 2, 3, 10, and 12 of Table I. Note that there are fundamental changes in the profiles of many components at places where garnet-bearing matrix becomes garnet-free. The reactions at this boundary act as sources and sinks to compensate for the differences in material transport caused by changes in chemical potential gradients due to the removal of the constraint provided by the Gibbs–Duhem relation of garnet.

The chemical potential profiles in fig. 7 also identify the major sources and sinks for each

component. A component is produced at a reaction site if the chemical potential profile forms an upward pointing 'peak' at the discontinuity that marks a reaction. If the profile forms a downward pointing 'valley' the component is consumed by the reaction. Examination of fig. 7 reveals several generalizations that can be made about sources and sinks in these rocks. Sillimanite segregations with or without garnet are always sources for K, Na, and Ca, while they are always sinks for Al. Staurolite pseudomorphs with or without garnet are always sources for Al and sinks for Ca and K. Staurolite pseudomorphs with garnet, sillimanite segregations without garnet, and matrix garnets that grow, are all Fe sinks while sillimanite segregations with garnets, staurolite pseudomorphs without garnets, and matrix garnets that dissolve, are all iron sources. The Mg sources in the rock are biotite-consuming reactions associated with garnet-bearing staurolite pseudomorphs and garnets growing in the matrix. The Mg sinks in the rock are biotite-producing reactions associated with garnet-free and garnet-bearing sillimanite segregations. Fe sources are Ti sinks and Fe sinks are Ti sources, because the transport direction of Ti through the matrix is always opposite that of Fe due to the Gibbs–Duhem relation for ilmenite.

Conclusions

This study has shown how irreversible thermodynamic models can be used to investigate the complex reaction mechanisms responsible for the evolution of textures in a rock as a metamorphic reaction proceeds. The models show that in any given rock, a single mineral (e.g. garnet) can be involved in local reactions that consume it, produce ir, or allow it to remain unchanged. The distribution of minerals in the rock at the time reaction begins and the nucleation site of the new mineral that appears in the rock are important controls on the local reactions that produce textures.

Many authors have pointed out that the ultimate control on reaction rates in metamorphic rocks is the amount that conditions in the rock differ from equilibrium conditions (e.g. Yardley, 1977; Fisher, 1978; Rubie, 1983; Walther and Wood, 1984; Ridley, 1985). Variation in the amount of overstepping of equilibrium conditions will have two effects: it strongly influences the number and type of nucleation sites for a new mineral and it affects the rates of transport that govern the rates of local reactions. At the beginning of a reaction these two effects are linked by a feed-back loop. After the first nuclei appear in the rock, reactions begin to take place that attempt to restore equilibrium. If local equilibrium is maintained, the rate of these

reactions will depend on the magnitude of the chemical potential gradients in the rock that link sites of local reactions and the magnitude of diffusion coefficients that relate the chemical potential gradients to material transport. For a prograde reaction, the magnitudes of the chemical potential gradients and diffusion coefficients depend upon the amount that the temperature in the rock exceeds the equilibrium temperature for the mineral assemblage that is present (the amount of overstepping). As long as the reaction rates cannot consume heat as fast as it is put into the rock, the temperature will continue to rise. This allows more nuclei to form and also increases the magnitude of chemical potential gradients and diffusion coefficients, causing an increase in the reaction rate that in turn increases the rate of heat consumption in the rock. Eventually, the heat consumption will equal or exceed the rate of heat input into the rock, resulting in a constant or falling temperature. If the temperature falls, the nucleation rate and the reaction rate will decrease because the overstepping has been lowered. This type of feedback should allow a steady state to be established, causing the temperature to remain relatively constant as the reactions consume about the same amount of heat that is added to the rock. If the temperature decrease has inhibited nucleation, then the only effect of small variations in the flow of heat into the rock will be to increase or decrease the magnitude of the chemical potential gradients and diffusion coefficients that control transport between reaction sites. This will keep the reaction rates in balance with the heat brought into the rock. Small variations in temperature under nearly steady-state conditions will have little effect on the textures that are produced, because the relative values of chemical potential gradients and diffusion coefficients between different components will remain essentially the same.

The effect of heating rate on nucleation, however, can profoundly influence the texture produced by a prograde reaction. Rocks that overstep the reaction slowly should allow a steady state temperature configuration to be established before many nuclei form. The result should be a rock containing a few large segregations. Rocks that change T and/or P rapidly should develop considerable overstepping before the transport rates can drive reactions fast enough to keep up with the heat input. This should form many nuclei, forming a rock with more abundant but smaller segregations (see Rubie, 1983, Table I for comparison of overstepping rates along different types of P, T trajectories). In some cases the textures that result can be quite different because of increased numbers of nucleation sites. For example, the texture shown in fig. 1b suggests

that the heating rate during prograde metamorphism on Elephant Mountain was relatively slow because sillimanite nucleated and grew only on one side of the garnet. In the Connemara schists, Yardley (1977) described a texture where sillimanite appears to nucleate entirely around garnets before much growth takes place, suggesting that the heating rate was faster than on Elephant Mountain. If the heating rate was even higher, one might expect to find textures that indicate abundant sillimanite nucleation on minerals with sites that require high activation energies and considerable overstepping. An example of this might be sillimanite pseudomorphs after staurolite rather than the sillimanite segregations and mica-rich pseudomorphs that are commonly found when sillimanite grows at the expense of staurolite in pelitic rocks. This type of phenomenon has not been adequately investigated, but it may be possible to draw significant conclusions about heating rates during prograde metamorphism based upon careful observations about the type of textures present in thin sections.

REFERENCES

Bailes, A. H., and McRitchie, W. D. (1978) The transition from low to high grade metamorphism in the Kisseynew Sedimentary Gneiss Belt, Manitoba, *Geol. Surv. Can. Paper 78-10,* 155–78.

Carmichael, D. M. (1969) On the mechanism of prograde metamorphic reactions in quartz-bearing pelitic rocks. *Contrib. Mineral. Petrol.* **20,** 244–67.

Fisher, G. W. (1975) The thermodynamics of diffusion-controlled metamorphic processes. In *Mass Transport Phenomena in Ceramics* (A. R. Cooper and A. H. Heuer, eds.), 111–22. Plenum, New York.

——(1977) Nonequilibrium thermodynamics in metamorphism. In *Thermodynamics in Geology* (D. G. Fraser, ed.), 381–403. Riedel, Boston.

——(1978) Rate laws in metamorphism. *Geochim. Cosmochim. Acta,* **42,** 1035–50.

Foster, C. T., Jr. (1975) *Diffusion Controlled Growth of Metamorphic Segregations in Sillimanite Grade Pelitic Rocks near Rangeley, Maine, U.S.A.* Ph.D. thesis, the Johns Hopkins University, Baltimore, Md.

——(1977) Mass transfer in sillimanite-bearing pelitic schists near Rangeley, Mains. *Am. Mineral.* **62,** 727–46.

——(1981) A thermodynamic model of mineral segregations in the lower sillimanite zone near Rangeley, Maine. Ibid. **66,** 260–77.

——(1982) Textural variation of sillimanite segregations. *Can. Mineral.* **20,** 379–92.

——(1983) Thermodynamic models of biotite pseudomorphs after staurolite. *Am. Mineral.* **68,** 389–97.

Guidotti, C. V. (1968) Prograde muscovite pseudomorphs after staurolite in the Rangeley–Oquossoc area, Maine. Ibid. **53,** 1368–76.

——(1970) The mineralogy and petrology of the transition from the lower to upper sillimanite zone in the Oquossoc area, Maine. *J. Petrol.* **11,** 277–336.

——(1974) Transition from staurolite to sillimanite zone, Rangeley Quadrangle, Maine. *Geol. Soc. Am. Bull.* **85,** 475–90.

Joesten, R. (1974) Local equilibrium and metasomatic growth of zoned calc–silicate nodules from a contact aureole, Christmas Mountains, Big Bend Regions, Texas. *Am. J. Sci.* **274,** 876–901.

——(1977) Evolution of mineral assemblage zoning in diffusion metasomatism. *Geochim. Cosmochim. Acta,* **41,** 649–70.

Nishiyama, T. (1983) Steady diffusion model for olivine-plagioclase corona growth. Ibid. **47,** 283–94.

Ridley, J. (1985) The effect of reaction enthalpy on the progress of a metamorphic reaction. In *Metamorphic Reactions: Kinetics, Textures and Deformation* (A. B. Thompson and D. C. Rubie, eds.), 80–97. Springer-Verlag, New York.

Rubie, D. C. (1983) Reaction-enhanced ductility: the role of solid–solid univariant reactions in deformation of the crust and mantle. *Tectonophys.* **96,** 331–52.

Walther, J. V., and Wood, B. J. (1984) Rate and mechanism in prograde metamorphism. *Contrib. Mineral. Petrol.* **88,** 246–59.

Yardley, B. W. D. (1977) The nature and significance of the mechanism of sillimanite growth in the Connemara schists, Ireland. Ibid. **65,** 53–8.